Zinc oxide nanoparticles synthesized using coffee leaf extract assisted with ultrasound as nanocarriers for mangiferin

Qiang Wang [a], Suhuan Mei [a], Perumal Manivel [a], Haile Ma [a,b], Xiumin Chen [a,b,c,*]

[a] School of Food and Biological Engineering, Jiangsu University, 301 Xuefu Road, Jingkou District, Zhenjiang, Jiangsu, 212013, PR China
[b] Institute of Food Physical Processing, Jiangsu University, 301 Xuefu Road, Jingkou District, Zhenjiang, Jiangsu, 212013, PR China
[c] International Joint Research Laboratory of Intelligent Agriculture and Agri-products Processing, Jiangsu University, Zhenjiang, 212013, China

ARTICLE INFO

ABSTRACT

Plant extracts have been widely used to green synthesize zinc oxide nanoparticles (ZnO NPs); however, how the combination of ultrasound and coffee leaf extract (CLE) affects the structure characteristics and the yield of ZnO NPs remains unknown. In this study, we used CLE to green synthesize ZnO NPs with the help of ultrasound. The highest yield ($43.59 \pm 0.13\%$) of ZnO NPs was obtained under the optimal processing conditions of pH = 8.0, mass ratio of coffee leaves to $C_4H_6O_4Zn \bullet 2H_2O = 1.71$, ultrasound time = 10 min, ultrasound frequency = 28/40 kHz, ultrasound power = 180 W, and synthesis temperature = 30 °C. The as-synthesized ZnO NPs were characterized by UV–Vis, SEM, EDX, TEM, FTIR, XRD, and zeta potential analyses. SEM and TEM analyses revealed that ZnO NPs synthesized using ultrasound-assisted method were spherical with an average particle size of 8.29 ± 1.38 nm, which was smaller than ZnO NPs synthesized without ultrasound treatment (10.48 ± 1.57 nm) and the chemically synthesized ZnO NPs (17.15 ± 2.84 nm). HPLC analysis showed that the phenolic compounds in coffee leaves, especially 5-CQA, were the main reductants and chelating agents for ZnO NPs synthesis. The synthesized ZnO NPs were used to load mangiferin, which was control released under pH 7.4 over 132 h. Our study provides an easy and eco-friendly method using CLE assisted with ultrasound for green synthesis of ZnO NPs which can be used as nanocarriers to control release of mangiferin.

1. Introduction

Zinc oxide nanoparticles (ZnO NPs) have received extensive attention due to their antibacterial functions and biomedical applications, especially used as anticancer drug and nanocarriers for anticancer drugs (Singh et al., 2020) because of their good biocompatibility, low-toxicity, chemical and thermal stability (Wang et al., 2020). Therefore, various chemical, physical, biological, and green synthesis approaches have been developed to synthesize ZnO NPs (Chen et al., 2009, 2010). The chemical method generally needs toxic reducing agents; therefore, it will cause safety issue and the environmental problem. However, plant extracts provide non-toxic and natural reducing, capping, and stabilizing agents for green synthesis of ZnO NPs (Basnet et al., 2018). Many researchers have used plant extracts, such as *Citrus sinensis* peel extract (Gao et al., 2020), *Dysphania ambrosioides* extract (Álvarez-Chimal et al., 2021) and leaf extract of *Mussaenda frondosa* L (Jayappa et al., 2020) to green synthesis of ZnO NPs. Except for plant extract, in the last two

decades, ultrasound has been extensively used in the green synthesis of metal or metal oxide NPs because the acoustic cavitation produces sheer force, agitation, elevated temperature, and free radicals, which lead to the synthesis of smaller NPs with narrower size distribution in a shorter time period without the use of reducing agents (Duan et al., 2015). Moreover, ultrasound can increase the yield of synthesized NPs (Sharifalhoseini et al., 2018). Therefore, using plant extract with the assistance of ultrasound is a promising green approach for the synthesis of ZnO NPs.

Coffee leaves are generally considered low- or no-value by-product of coffee plants. They are discarded in the land field when trim the branches off coffee trees, thus leading to the waste of resources and causing sever environmental problem. However, coffee leaves are rich in phytochemicals such as chlorogenic acids, mangiferin, rutin, amino acids, proteins, and carbohydrates, therefore, coffee leaves have been made into coffee leaf tea or used as ethnic medicine in the countries such as Ethiopia, Indonesia, Sumatra, Uganda, Nicaragua (Chen, 2019). The biologically active compounds in coffee leaves are excellent reductants,

Abbreviation

CLE	coffee leaf extract
5-CQA	5-caffeoylquinic acid
CQAs	caffeoylquinic acid
3,4-diCQA	3,4-dicaffeoylquinic acid
3,5-diCQA	3,5-dicaffeoylquinic acid
4,5-diCQA	4,5-dicaffeoylquinic acid
EDX	energy dispersive X-ray
UV–Vis	ultraviolet–visible spectroscopy
FTIR	Fourier transform infrared spectroscopy
HPLC	high performance liquid chromatography
NPs	nanoparticles
N-US	non-ultrasound-assisted synthesis
PBS	phosphate buffer saline;
SEM	scanning electron microscopy
TEM	transmission electron microscope
TFA	trifluoroacetic acid
TPC	total phenolic content
US	ultrasound-assisted synthesis
XRD	X-ray diffraction

capping agents, and stabilizers that can be used to green synthesis of NPs. Coffee leaf extract (CLE) has been used to synthesize reduced graphene oxide nanocomposite which possessed antioxidant and anti-inflammatory activities (Perera et al., 2021). To our best knowledge, there is no research using coffee leaves to synthesize ZnO NPs. Therefore, it would be interesting to synthesize ZnO NPs using CLE to produce value-added products.

Mangiferin (1,3,6,7-tetrahydroxyxanthone-C2-β-d glucoside) is a C-glycosylated xanthone that possesses various bioactivities, including antioxidant, anti-inflammatory, antivirus, and anticancer capacities (Mei et al., 2021a). However, the poor solubility and bioavailability of mangiferin results in the low efficacy in human body. To solve this problem, scientists have made great efforts to improve the solubility and bioavailability of mangiferin through various methods such as structural modification, loading mangiferin in the nano/micro carriers, or administration of mangiferin with other components (Mei et al., 2021b). ZnO NPs have been used as carriers for doxorubicin, curcumin, quercetin, camptothecin, isotretinoin, daunorubicin, barberine, and chlorogenic acid to enhance the cytotoxicity and pH-dependent control release of drug (Singh et al., 2020). However, mangiferin loaded ZnO NPs have not been reported in the literature yet.

In the present study, we used CLE to synthesize ZnO NPs with the assistance of ultrasound and investigated the impacts of different ultrasonic conditions, including pH, mass ratio of coffee leaves to $C_4H_6O_4Zn{\bullet}2H_2O$, ultrasound time, frequency, power and temperature on the yield of ZnO NPs. Multiple-spectrometry and microscopy methods, including ultraviolet–visible spectroscopy (UV–Vis), Fourier transform infrared spectroscopy (FTIR), scanning electron microscopy (SEM), energy dispersive X-ray analysis (EDX), transmission electron microscope (TEM), and X-ray diffraction (XRD) were used to characterize and compare the structures of ZnO NPs synthesized using CLE with and without ultrasound treatment and the conventional chemical method. The change in phytochemical profile of CLE was assessed to evaluate the key reductants for synthesis of ZnO NPs. Finally, ZnO NPs were used to encapsulate mangiferin and the release of mangiferin under pH 7.4 was also investigated. We aim to provide a green and easy way to synthesize ZnO NPs using CLE assisted with ultrasound and use ZnO NPs as carriers for mangiferin.

2. Materials and methods

2.1. Materials

$C_4H_6O_4Zn{\bullet}2H_2O$ was purchased from Shanghai Aladdin Biochemical Technology Co. Ltd. (Shanghai, China). Folin-Ciocalteu's phenol reagent was purchased from Beijing Solarbio Science & Technology Co. Ltd. (Beijing, China). Gallic acid and $NaBH_4$ were purchased from Sinopharm Chemical Reagent Co. Ltd. (Beijing, China). Phytochemical standards, including mangiferin, rutin, trigonelline, caffeine and chlorogenic acids (5-CQA: 5-caffeoylquinic acid; 3,4-diCQA: 3,4-dicaffeoylquinic acid; 3,5-diCQA: 3,5-dicaffeoylquinic acid; 4,5-diCQA: 4,5-dicaffeoylquinic acid) were purchased from Chengdu Must Bio-Technology Co. Ltd. (Chengdu, China). The fresh leaves of *Coffea arabica* were obtained from Hougu Coffee Plantation in Mangshi, Dehong County, Yunnan Province, China. All other reagents are analytical grade and purchased from Sinopharm Chemical Reagent Co. Ltd. (Zhenjiang, China).

2.2. Preparation of coffee leaf extract

Fresh coffee leaves were freeze-dried, ground and passed through a 60-mesh sieve. Coffee leaf powders (20 g) were extracted twice with 400 mL boiling ddH₂O for 20 min in a boiling water bath. The extracts were filtered and the supernatant was stored at 4 °C for further use.

2.3. Ultrasound-assisted green synthesis of ZnO NPs using coffee leaf extract

All the ultrasound treatments were performed in a multi-frequency power ultrasound device designed by Dr. Haile Ma's group (Jiangsu University) (Ji et al., 2021). The effects of pH (7.0, 7.5, 8.0, 8.5, 9.0), mass ratio of coffee leaves to $C_4H_6O_4Zn{\bullet}2H_2O$ (0.23, 0.46, 0.68, 0.91, 1.14, 1.37, 1.71, 2.28), ultrasound time (10, 20, 30, 40, 50 min), ultrasound frequency (single-frequency (20, 28, 40 kHz), dual-frequency (20/28, 20/40, 28/40 kHz) and triple-frequency (20/28/40 kHz), ultrasound power (60, 120, 180, 240, 300 W) and temperature (20, 25, 30, 40, 50, 60, 70 °C) on the yield of ZnO NPs were investigated using one factor at a time experimental design.

Different volume of CLE was mixed with $C_4H_6O_4Zn{\bullet}2H_2O$ (0.1 mol/L) in 100 mL total volume and then adjusted to different pH by addition of HCl (1 mol/L) or NaOH (1 mol/L) solution. After reaction, the mixture was centrifuged at $11610{\times}g$ for 20 min. The precipitate was washed with ultrapure water five times followed by dried in an oven at 80 °C for 9 h and then calcined at 400 °C for 2 h. ZnO NPs were also synthesized using CLE without ultrasound treatment under the optimal conditions. The yield of ZnO NPs was calculated as follow:

$$\text{Yield}(\%) = \frac{\text{Weight of ZnO NPs}}{\text{Weight of } C_4H_6O_4Zn} \times 100 \qquad (1)$$

2.4. Chemical synthesis of ZnO NPs

A chemical method was also used to synthesize ZnO NPs according the method described by Khalil and Alqahtany (2020). Briefly, 50 mL (0.2 mol/L) $C_4H_6O_4Zn{\bullet}2H_2O$ solution and 50 mL 0.2 mol/L $NaBH_4$ solution were agitated for 1 h, and then settled overnight. After centrifugation and washing, the precipitates were dried at 80 °C for 9 h, then calcined at 400 °C for 2 h.

2.5. Measurement of total phenolic content

Total phenolic content (TPC) in the CLE before and after reaction was measured according to Chen's method (Chen et al., 2017). The percentage change of TPC (ΔTPC, %) before and after synthesis was calculated as follow:

$$\Delta TPC \ \ (\%) = \frac{TPC \ \ before \ \ reaction - TPC \ \ after \ \ reaction}{TPC \ \ before \ \ reaction} \times 100 \quad (2)$$

2.6. Analysis of phytochemical composition of coffee leaf extract

The phytochemicals in CLE were analyzed using HPLC according to the method described by Chen et al. (2018).

2.7. Characterization of ZnO NPs

ZnO NPs synthesized by the above three methods were characterized by multi-spectroscopy and microscopy methods. UV–Vis spectrum (200–800 nm) of ZnO NPs suspension was measured using a spectrometer (UV-1601, PerkinElmer, USA). The zeta potential of ZnO NPs was measured using a particle size analyzer (Litesizer 500, Anton Paar, USA). TEM (HT7800, Hitachi High-Tech Group, Japan) and SEM (JSM-7800F, JEOL, Japan) equipped with an EDX spectrometer were used to observe the size, morphology, and the elements present in ZnO NPs. The Image J software was used to calculate the average particle size of ZnO NPs based on the average of 100 NPs. XRD was recorded using an X-ray diffractometer (D8 ADVANCE, BRUKER, Germany) in the 2θ range of 20–80° at 40 kV and 40 mA with the scanning speed 4°/min to show the crystallinity of ZnO NPs. FTIR spectrometer (Nicolet iS50, Thermo Fisher Scientific, USA) was used to identify the surface capping groups of the synthesized ZnO NPs.

2.8. Loading of mangiferin on ZnO NPs

ZnO NPs (50 mg) synthesized under optimal ultrasound conditions were mixed with 50 mL 0.2 mg/mL mangiferin in 50% methanol solution. The mixture was stirred for 12 h in the darkness. The precipitate was washed with ultrapure water four times to remove physically adsorbed mangiferin. Mangiferin loaded ZnO NPs (MGF-ZnO NPs) were freeze-dried. The absorbance of mangiferin solution was measured by a UV spectrophotometer (Shanghai Metash Instruments Co. Ltd., Shanghai, China) at 257 nm and the concentration was calculated based on the mangiferin standard curve. The encapsulation and loading efficiencies of mangiferin were calculated as follows:

$$Encapsulation \ \ efficiency \ \ (\%) = \frac{Added \ \ mangiferin - Mangiferin \ \ left \ \ in \ \ the \ \ solution}{Added \ \ mangiferin} \times 100 \quad (3)$$

$$Loading \ \ efficiency \ \ (\%) = \frac{Added \ \ mangiferin - Mangiferin \ \ left \ \ in \ \ the \ \ solution}{Weight \ \ of \ \ MGF - ZnO \ \ NPs} \times 100 \quad (4)$$

2.9. Release of mangiferin from ZnO NPs

The *in vitro* release behavior of mangiferin from ZnO NPs was investigated by dialysis. MGF-ZnO NPs (20 mg) were mixed with 20 mL pH 7.4 phosphate buffer solution (PBS) in a dialysis bag with a molecular cut off 8000 Da. The dialysis bag was placed in a beaker containing 80 mL PBS solution and shaken at 100 rpm under 37 °C. An aliquot of 10 mL PBS solution was taken and replaced with 10 mL fresh PBS every 12 h until 132 h. The cumulative release at different time points were calculated using equation (5):

$$Drug \ \ released(\%) = \frac{Accumulated \ \ amount \ \ of \ \ mangiferin \ \ released}{Initial \ \ amount \ \ of \ \ mangiferin} \times 100 \quad (5)$$

2.10. Statistical analysis

Data were expressed as means ± SD. The statistically significant difference was analyzed by one-way analysis of variance (ANOVA) with Tukey's post hoc test using MINITAB 17 software (Minitab Inc., State College, PA, USA) or student's t-test using Excel. A $P < 0.05$ denotes significant difference. All the experiments were performed in triplicate.

3. Results and discussion

3.1. The effects of ultrasonic conditions on the yield of ZnO NPs

3.1.1. The effect of pH

Table 1 presents the impacts of pH, mass ratio, and ultrasound time, frequency, power, and temperature on the yield of ZnO NPs. The results indicated that the yield of ZnO NPs was gradually increased from pH 7.0 to 8.0 and then decreased between pH 8.0 and 9.0. The highest yield (36.26 ± 0.89%) of ZnO NPs was observed at pH 8.0, indicating that the alkaline condition was more favorable to the synthesis of ZnO NPs than acidic or neutral condition. Alia et al. (2016) studied the influence of pH (5.0–10.0) on the formation of ZnO NPs using *Aloe vera* skin extract and found that the optimum pH required for the biosynthesis of ZnO NPs was also 8.0, which was similar to our findings. Hence, in the following experiments, ZnO NPs were synthesized at pH 8.0.

3.1.2. The effect of mass ratio of coffee leaves to $C_4H_6O_4Zn \bullet 2H_2O$

Mass ratio had a significant impact on the yield of ZnO NPs. With the increasing content of CLE, the yield of ZnO NPs increased gradually (Table 1). The maximum yield of 40.43 ± 0.99% was observed in the reaction mixture with the mass ratio of 1.71 : 1, which was due to the increase in the concentration of CLE. The increased phenolic compounds and other plant components such as amino acids, proteins, and carbohydrates in CLE could effectively support the reduction reaction and function as stabilizers and capping reagents (Basnet et al., 2018). Moreover, the increase of CLE can also improve the chelation between phenolic compounds and Zn^{2+}, thereby enhancing the yield of ZnO NPs after calcination (Nava et al., 2017). Similar result was reported by Jamdagni et al. (2018) who found that addition of flower extract of *Nyctanthes arbor-tristis* from 0.25 mL to 1 mL gradually increased the yield of ZnO NPs, while further increased the extract volume to 2 mL resulted in a declined yield of ZnO NPs.

3.1.3. The effect of ultrasound time

As shown in Table 1, ultrasound time did not significantly affect the yield of ZnO NPs. After 10 min ultrasonication, the yield of ZnO NPs

Table 1
The impacts of ultrasonic conditions on the yield of ZnO NPs.

Ultrasonic conditions	Levels	Yield/%
pH[a]	7.0	4.58 ± 0.31^d
	7.5	24.99 ± 0.33^c
	8.0	36.26 ± 0.89^a
	8.5	33.94 ± 0.32^b
	9.0	34.08 ± 1.58^{ab}
Mass ratio[b]	0.23 : 1	34.49 ± 0.38^e
	0.46 : 1	36.00 ± 0.18^{de}
	0.68 : 1	36.26 ± 0.89^{cd}
	0.91 : 1	39.20 ± 0.42^{ab}
	1.14 : 1	39.64 ± 0.31^{ab}
	1.37 : 1	39.83 ± 0.62^a
	1.71 : 1	40.43 ± 0.99^a
	2.28 : 1	37.98 ± 0.59^{bc}
Time[c] **(min)**	10	39.44 ± 1.40^a
	20	39.51 ± 0.25^a
	30	40.43 ± 0.99^a
	40	40.91 ± 1.04^a
	50	40.67 ± 0.43^a
Frequency[d] **(kHz)**	20	40.42 ± 1.7^{ab}
	28	40.78 ± 0.73^{ab}
	40	39.44 ± 1.40^{ab}
	20/28	38.36 ± 0.77^{bc}
	20/40	40.63 ± 0.69^{ab}
	28/40	41.40 ± 0.58^a
	20/28/40	36.62 ± 0.06^c
Power[e] **(W)**	60	38.82 ± 0.37^b
	120	40.13 ± 0.66^{ab}
	180	41.40 ± 0.58^a
	240	40.88 ± 0.04^a
	300	41.02 ± 0.62^a
Temperature[f] **(°C)**	20	41.34 ± 0.21^b
	25	41.56 ± 0.17^b
	30	43.59 ± 0.13^a
	40	41.83 ± 0.25^{ab}
	50	41.40 ± 0.58^b
	60	41.66 ± 1.58^{ab}
	70	43.23 ± 0.82^{ab}

Data were expressed as mean $\pm$ SD; Means do not share letters denote significant difference at P < 0.05.

[a] The ultrasound conditions are as follows: mass ratio = 0.68, ultrasound time = 30 min, ultrasound frequency = 40 kHz, ultrasound power = 180 W, synthesis temperature = 50 °C, pH = 7.0, 7.5, 8.0, 8.5, 9.0.

[b] The ultrasound conditions are as follows: pH = 8.0, ultrasound time = 30 min, ultrasound frequency = 40 kHz, ultrasound power = 180 W, synthesis temperature = 50 °C, mass ratio = 0.23, 0.46, 0.68, 0.91, 1.14, 1.37, 1.71, 2.28.

[c] The ultrasound conditions are as follows: pH = 8.0, mass ratio = 1.71, ultrasound frequency = 40 kHz, ultrasound power = 180 W, synthesis temperature = 50 °C, ultrasound time = 10, 20, 30, 40, 50 min.

[d] The ultrasound conditions are as follows: pH = 8.0, mass ratio = 1.71, ultrasound time = 10 min, ultrasound power = 180 W, synthesis temperature = 50 °C, ultrasound frequency = 20, 28, 40, 20/28, 20/40, 28/40, 20/28/40 kHz.

[e] The ultrasound conditions are as follows: pH = 8.0, mass ratio = 1.71, ultrasound time = 10 min, ultrasound frequency = 28/40 kHz, synthesis temperature = 50 °C, ultrasound power = 60, 120, 180, 240, 300 W.

[f] The ultrasound conditions are as follows: pH = 8.0, mass ratio = 1.71, ultrasound time = 10 min, ultrasound frequency = 28/40 kHz, ultrasound power = 180 W, synthesis temperature = 20, 25, 30, 40, 50, 60, 70 °C.

reached $39.44 \pm 1.40\%$, which was not significantly different from the highest yield of $40.91 \pm 1.04\%$ observed at 40 min. The synthesis of ZnO NPs using plant extracts without ultrasound generally takes much longer time, ranging from several hours to overnights. Alia et al. (2016) synthesized ZnO NPs using *Aloe vera* extract through vigorously stirring for 3 h at 60 °C. Selim et al. (2020) used *Deverra tortuosa* aqueous extract to synthesize ZnO NPs overnight. Our result indicated that with the help of ultrasound, the reaction time was significantly decreased. The reason is that the acoustic cavitation produces the hot spots with high temperatures (~5000 K) and high pressure (~150 MPa), sheer force, agitation, and free radicals, which accelerate the reaction rate, thereby decreasing the reaction time (Duan et al., 2015). From the economic point of view,

longer ultrasound time causes more energy consumption, therefore the ultrasound time was selected as 10 min for subsequent experiments.

3.1.4. The effect of ultrasound frequency

We investigated seven ultrasound frequency modes including single, double and triple frequencies on the yield of ZnO NPs. The results (Table 1) showed that there was no significant difference in the yield of ZnO NPs when synthesized under single-frequency of 20, 28, 40 kHz. Dual-frequency of 28/40 kHz increased the yield to a maximum level of $41.40 \pm 0.58\%$; however, triple-frequency 20/28/40 kHz treatment caused a minimum yield of $36.62 \pm 0.06\%$. It is well known that the tremendously high temperature and pressure produced during acoustic cavitation leads to various mechanical and chemical impacts to the reaction systems. The collapsing bubble results in the production of hydrogen and hydroxyl radicals which possess reducing and oxidizing capacities (Makino et al., 1983). The yield of these primary radicals is strongly affected by the ultrasound frequency, cavitation intensity, power intensity, collapse temperature, thereby influencing the rate of sonochemical reactions (Majumdar, 2019). The reason that the yield of ZnO NPs was greatest under 28/40 kHz frequency treatment could be due to the optimal mechanical and chemical effects under this condition, thereby speeding up the sonochemical reaction rate. However, the reason that triple frequency of 20/28/40 leaded to the lowest yield needs further study. The dual frequency of 28/40 kHz was used in the following experiments.

3.1.5. The effect of ultrasound power

The yield of ZnO NPs was increased when ultrasound power increased from 60 to 180 W; however, further increasing the ultrasound power to 300 W did not show any significant changes in the yield (Table 1). The observed higher yield of $41.40 \pm 0.58\%$ at 180 W could be due to the increasing generation of free radicals as the power intensity increase, which can increase the sonochemical reaction rate (Majumdar, 2019). However, higher power might not be conducive to the cavitation effect of ultrasound, as too many cavitation bubbles would interfere with the propagation of sound waves, thereby affecting the synthesis of ZnO NPs. Pal et al. (2009) found that the yield of ZnO NPs was greatly reduced when the ultrasound power was greater than 350 W, and the porous ZnO structure could not be produced when ultrasound power lower than 100 W. Therefore, both our and previous research indicated that ultrasound power is a critical factor that affects the yield and structural characteristics of ZnO NPs. The optimal ultrasound power of 180 W was used for the next experiments.

3.1.6. The effect of synthesis temperature

Temperature is one of the main factors that affects the nucleation and growth of NPs crystals (Bandeira et al., 2020). As shown in Table 1, when temperature increased from 20 to 30 °C, the yield of ZnO NPs was significantly enhanced; however further increase of the temperature resulted in a decrease of the yield. The maximum yield ($43.59 \pm 0.13\%$) of ZnO NPs was observed at the ultrasound temperature of 30 °C, which was similar to the yield of ZnO NPs synthesized at 70 °C. The reason might be that the change of temperature could affect the cavitation effect and the rate of the synthesis reaction. Omran et al. (2018) studied the effect of different reaction temperatures (20–60 °C) on the synthesis of AgNPs using *Citrus sinensis* peels extracts and they found the optimum temperature for the maximum production of AgNPs was 40 °C.

Based on the experimental results, the optimum conditions were determined as follows: pH = 8.0, mass ratio = 1.71, ultrasound time = 10 min, ultrasound frequency = 28/40 kHz, ultrasound power = 180 W, synthesis temperature = 30 °C. ZnO NPs obtained under optimum conditions were used for characterization and subsequent experiments.

Table 2
Total phenolic content and phytochemical compositions in the coffee leaf extract before and after ZnO NPs synthesis.

Treatment		TPC (mg gallic acid/g leaf)	Phytochemical compositions (μg/mL)							
			Mangiferin	Rutin	Trigonelline	Caffeine	5-CQA	3,4-diCQA	3,5-diCQA	4,5-diCQA
US[a]	Before	79.82 ± 6.38*	95.84 ± 2.92*	78.73 ± 2.78*	244.78 ± 7.55*	192.15 ± 9.30*	355.79 ± 12.23*	28.65 ± 0.83*	53.95 ± 1.70*	19.27 ± 0.29*
	After	1.44 ± 0.39	4.45 ± 0.29	ND	156.67 ± 13.13	140.19 ± 8.92	1.38 ± 2.39	ND	ND	ND
	Change (%)	98.16 ± 0.65†	95.36 ± 0.16	100.00 ± 0.00	36.06 ± 3.60†	27.08 ± 1.13†	99.62 ± 0.65†	100.00 ± 0.00	100.00 ± 0.00	100.00 ± 0.00
N-US[b]	Before	79.82 ± 6.38#	95.84 ± 2.92#	78.73 ± 2.78#	244.78 ± 7.55#	192.15 ± 9.30#	355.79 ± 12.23#	28.65 ± 0.83#	53.95 ± 1.70#	19.27 ± 0.92#
	After	2.24 ± 0.10	4.51 ± 0.00	ND	176.59 ± 3.60	156.67 ± 3.96	4.07 ± 0.11	ND	ND	ND
	Change (%)	97.10 ± 0.25	95.29 ± 0.15	100.00 ± 0.00	27.79 ± 3.50	18.47 ± 2.06	98.85 ± 0.02	100.00 ± 0.00	100.00 ± 0.00	100.00 ± 0.00

* Denote significant differences ($P < 0.05$) between samples before and after ZnO NPs synthesis under ultrasound treatment.
\# Denote significant differences ($P < 0.05$) between samples before and after ZnO NPs synthesis without ultrasound treatment.
† Denote significant differences ($P < 0.05$) between the changes of samples with and without ultrasound treatment.
Data were shown as means ± SD.
ND = Not detectable.
[a] ZnO NPs synthesis with ultrasound treatment under optimum conditions.
[b] ZnO NPs synthesis without ultrasound treatment under optimum conditions.

3.2. Comparison of chemical, ultrasound-assisted and non-ultrasound-assisted synthesis of ZnO NPs

We also synthesized ZnO NPs under the above optimum conditions using CLE without ultrasound treatment to elucidate the impacts of ultrasound on the structure characteristics and the yield of ZnO NPs. The results showed that the yield of ZnO NPs synthesized without ultrasound treatment (41.45 ± 0.34%) was significantly ($P < 0.05$) lower than that prepared with ultrasound treatment (43.59 ± 0.13%). This finding is possible due to ultrasound accelerating the reaction rate, thus increasing the yield of ZnO NPs. Moreover, a conventionally chemical method was also used to synthesize ZnO NPs and the yield (24.79 ± 0.50%) was significantly lower compared with the green synthesis of ZnO NPs using CLE. The plausible reasons are that firstly, phytochemicals in CLE were encapsulated in ZnO NPs, thereby increasing the yield; secondly, the reaction conditions in chemical and green synthesis methods are different, thus influencing the yield of ZnO NPs.
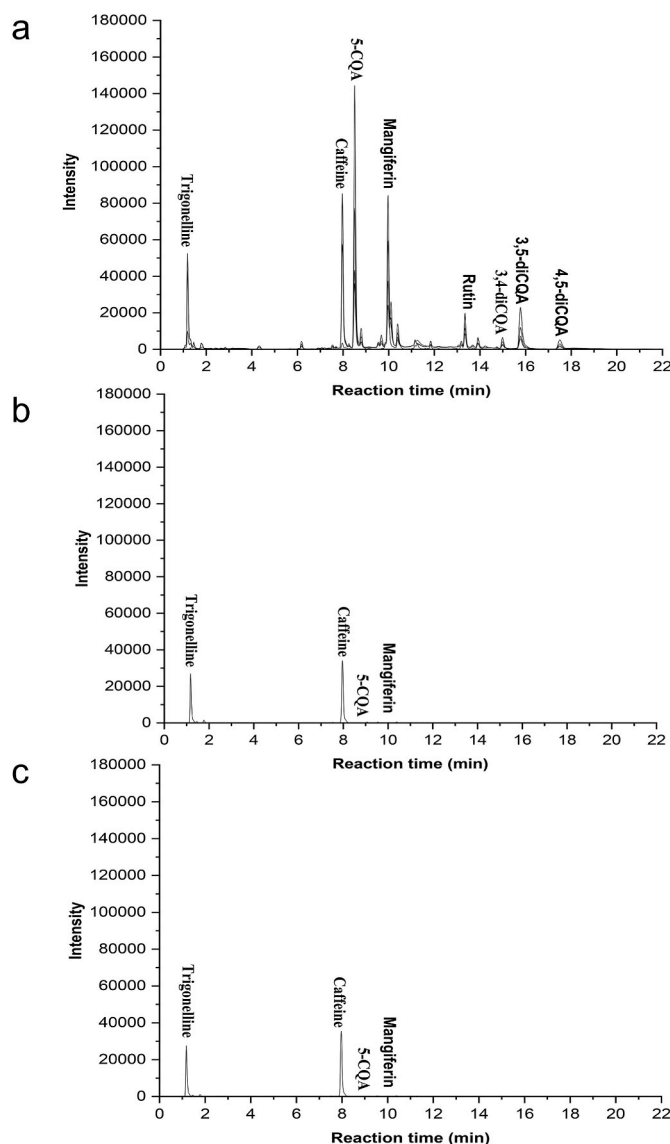
Fig. 1. HPLC chromatograph of phytochemical compositions in reaction mixture at 257 nm **a**, Before synthesis; **b**, After ultrasound-assisted synthesis; **c**, After non-ultrasound-assisted synthesis.

3.3. The change of TPC and phytochemical compositions in the reaction systems

The change of TPC and phytochemical compositions in the reaction mixture with (US) and without (N-US) ultrasound treatment are shown in Table 2. The decrease of TPC was $98.16 \pm 0.65\%$ and $97.10 \pm 0.25\%$, respectively, indicating that most of the phenolic compounds were used as reductants or chelators for the synthesis of ZnO NPs and the consumption of phenolic compounds in the US reaction system was greater than that of N-US reaction system. We further elucidated the changes of the phytochemical compositions in both reaction systems (Fig. 1 and Table 2). 5-CQA (355.79 ± 12.23 μg/mL) was the most abundant phenolic compounds in CLE. Similar to the change of TPC, the phenolic compounds, including mangiferin, rutin, 5-CQA, 3,4-diCQA, 3,5-diCQA and 4,5-diCQA were almost completely consumed in both reaction systems (89.11%–100%). The concentrations of these phenolic compounds in both US and N-US systems were not significantly different. The decrease of trigonelline and caffeine was to a lesser extent compared with that of phenolic compounds. In the US reaction system, trigonelline and caffeine were reduced $36.06 \pm 3.60\%$ and $27.08 \pm 1.13\%$, respectively, which were significantly higher than that of N-US reaction system ($27.79 \pm 3.50\%$ and $18.47 \pm 2.06\%$, respectively). It has been reported earlier that the flavonoids and phenolic compounds participate in the reduction, formation and stabilization process of metal NPs and metal oxide NPs (Ahmed et al., 2017). Our results suggested that polyphenolic compounds may involve in the reduction of Zn^{2+}, and 5-CQA plays a major role in the reduction. The contribution of trigonelline and caffeine to the ZnO NPs synthesis was much lesser compared with phenolic compounds because they are alkaloids that possess lower reducing power.

Although numerous research reported the green synthesis of ZnO NPs using plant extracts, the underlying mechanisms of the formation of ZnO NPs remain unknown. The possible mechanisms summarized by Bandeira et al. (2020) and Basnet et al. (2018) included: 1) The phytochemicals such as flavonoids, chlorogenic acids, limonoids, and carotenoids in the plant extract function as chelators that can chelate Zn^{2+} to form metal coordinated complexes that can be hydrolyzed to produce Zn $(OH)_2$ which is further degraded to form ZnO NPs after calcination (Nava et al., 2017; Matinise et al., 2017); 2) The antioxidant in plant extract, such as phenolic compounds can reduce Zn^{2+} to metallic zinc (Zn^0) which can be oxidized to form ZnO nuclei by the dissolved oxygen present in the solution (Gupta et al., 2018; Sutradhar and Saha, 2016). However, further research needs to be done to confirm these assumptions.

3.4. Characterization of ZnO NPs

3.4.1. UV–visible absorption spectrum analysis

The recombination changes of the free electrons of metal NPs when they resonate with light waves would produce surface plasmon resonance (SPR) absorption bands (Sachdeva et al., 2021). ZnO NPs produce characteristic absorption peaks between 310 and 380 nm due to the SPR band of NPs (Fu and Fu, 2015). Fig. 2 shows the successful synthesis of ZnO NPs using CLE with or without ultrasound treatment. The ZnO NPs synthesized using US and N-US method exhibited maximum absorption (λ_{max}) at 376 nm, whereas the chemically synthesized ZnO NPs showed its maximum absorption peak at 346 nm. The UV–Vis spectrum can be used to characterize NPs since the optical properties of NPs are sensitive to their size, shape, aggregation, and components (Wang and Cao, 2020). It is known that the size of Ag and Au nanoparticles is positively correlated with the maximum extinction wavelength, however, this correlation is weak for the metal oxide, graphite, and polystyrene NPs (Wang and Cao, 2020). Therefore, the red shift of ZnO NPs synthesized using CLE was possible due to the encapsulation or loading of phytochemicals and other impurity components in ZnO NPs. Sangeetha et al. (2011) found that the increase of the *aloe barbadensis miller* leaf extract concentration from 5% to 50% caused the continuous increase of λ_{max}. When the concentration was greater than 15%, λ_{max} of the ZnO NPs was higher than that of synthesized by chemical method, which was similar to our result.

3.4.2. SEM and EDX analysis

The morphological characteristics of as-prepared ZnO NPs were recorded using SEM. Fig. 3(a–c) showed that ZnO NPs prepared by all three methods were approximately spherical in shape and tended to aggregate into larger particles. The observed agglomeration might be caused by the drying process (Mohanpuria et al., 2008) or by the surface charge of ZnO NPs. After loading mangiferin on the surface of ZnO NPs, the aggregation degree of NPs was reduced and individual NPs could be seen more clearly.

EDX spectrum in Fig. 3 (a3-d3) showed strong signal peaks of Zn and O at 1 keV and 0.5 keV, respectively, indicating the formation of ZnO NPs (Chaudhuri and Malodia, 2017). Fig. 3d showed a strong peak at 0.28 keV, which represents the presence of C (Osuntokun et al., 2019), indicating that mangiferin was successfully loaded on the ZnO NPs.

3.4.3. TEM analysis

The TEM image of ZnO NPs synthesized by ultrasound-assisted method displayed agglomerated clusters of NPs with average particle size of 8.29 nm (Fig. 4a), which was significantly smaller than that of NPs synthesized without ultrasound treatment (10.48 nm, Fig. 4b). Fig. 4c showed hexagonal ZnO NPs were formed using chemical method and the average particle size was 17.15 ± 2.84 nm, which was significantly bigger than ZnO NPs synthesized using CLE. This observation was possible due to the phytochemicals in CLE acting as capping and stabilizing agents (Basnet et al., 2018), which lead to the production of smaller size ZnO NPs. Sangeetha et al. (2011) also found that green synthesis of ZnO NPs using *aloe barbadensis miller* leaf extract significantly reduced the particle size compared with chemical method. Notably, the ultrasound-assisted synthesized ZnO NPs exhibited a smaller sized and better dispersed NPs compared with NPs synthesized without ultrasound treatment due to the agitation effect of ultrasound (Pinjari et al., 2016).

3.4.4. XRD analysis

XRD analysis showed that the observed diffraction peaks of as-prepared ZnO NPs using US, N-US, and chemical methods were similar (Fig. 5). Diffraction peaks appeared at 2θ values around 32.51°, 34.62°, 36.94°, 48.21°, 57.83°, 63.49°, 67.87°, 70.65°, 73.01° and
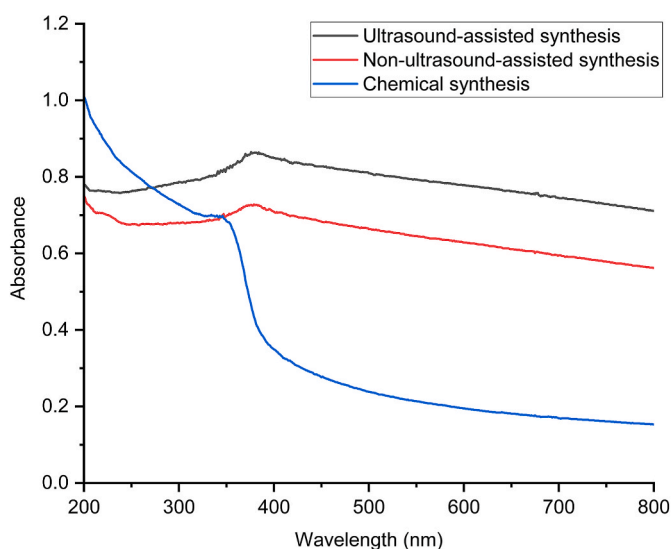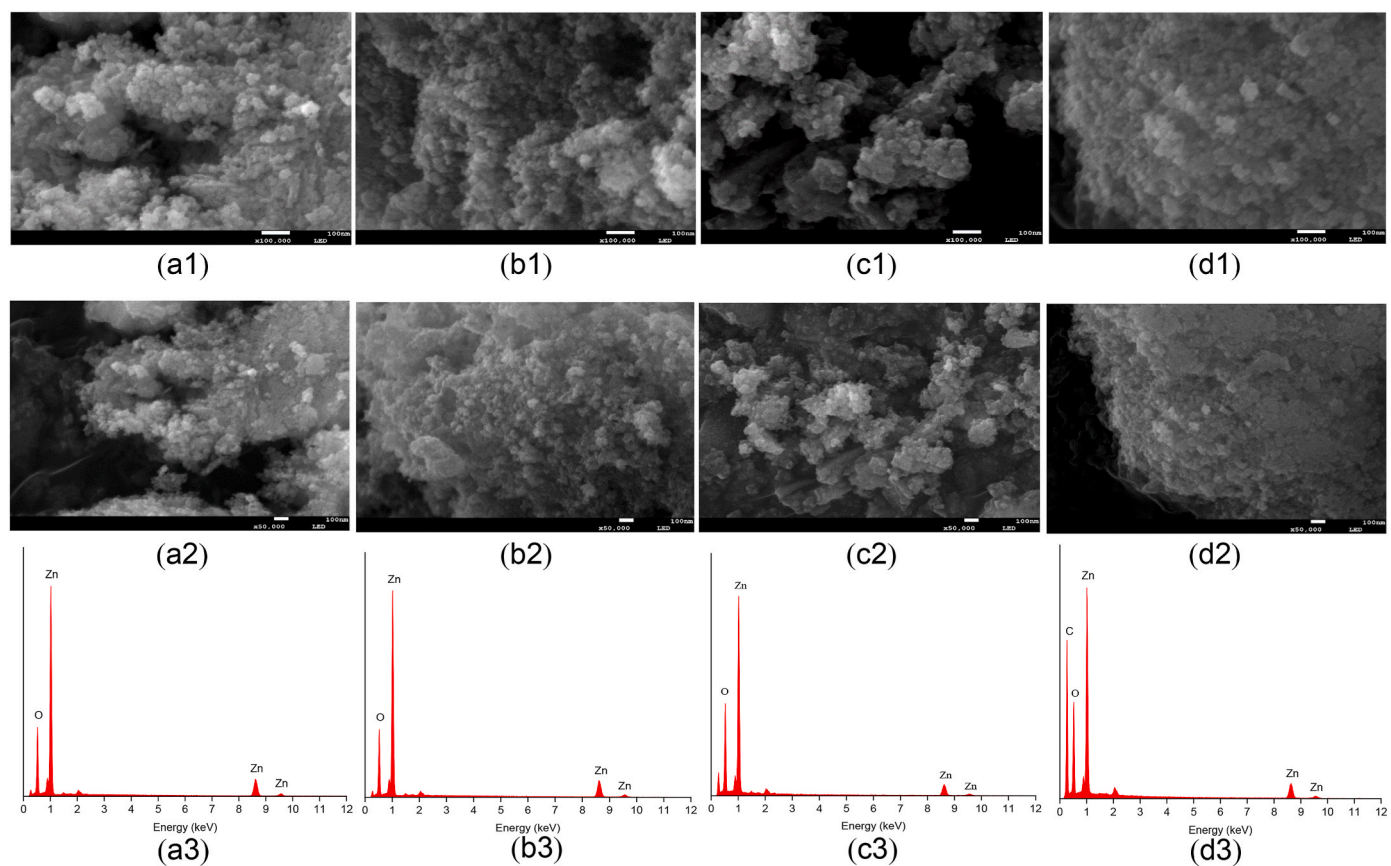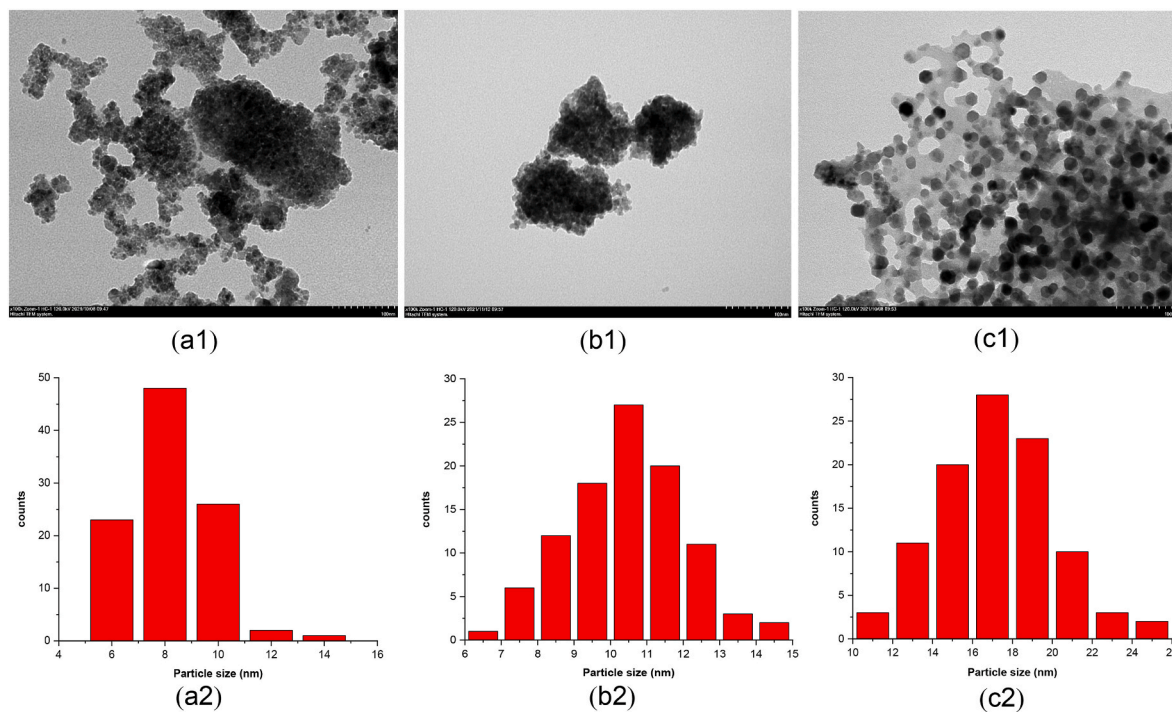
Fig. 2. UV–Vis spectrum of the ZnO NPs.

Fig. 3. SEM images and EDX spectrum of ZnO NPs. **a**, Ultrasound-assisted synthesis using coffee leaf extract; **b**, Non-ultrasound-assisted synthesis using coffee leaf extract; **c**, Chemical synthesis; **d**, Mangiferin loaded ZnO NPs. **a1**, **b1**, **c1**, **d1** with magnification 100,000×; **a2**, **b2**, **c2**, **d2** with magnification 50,000×. **a3**, **b3**, **c3**, **d3** are EDX spectrum of the corresponding ZnO NPs.

Fig. 4. TEM images and the size distribution of ZnO NPs. **a**, Ultrasound-assisted synthesis using coffee leaf extract; **b**, Non-ultrasound-assisted synthesis using coffee leaf extract; **c**, Chemical synthesis. **1** represents TEM images and **2** represents frequency distribution histograms of size.
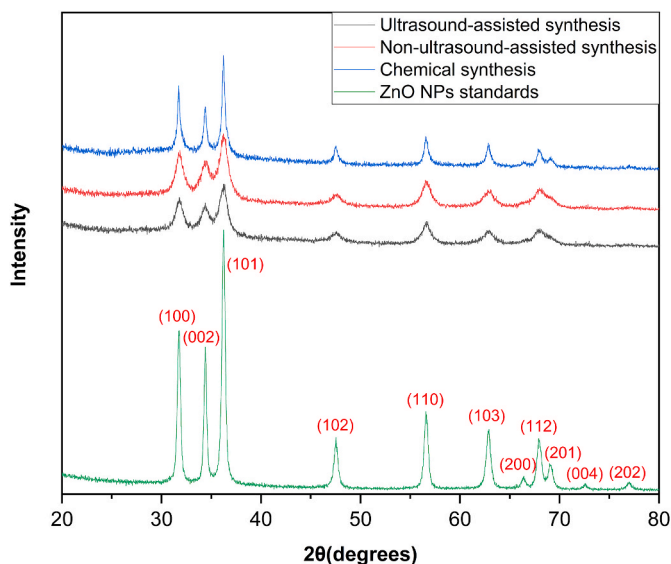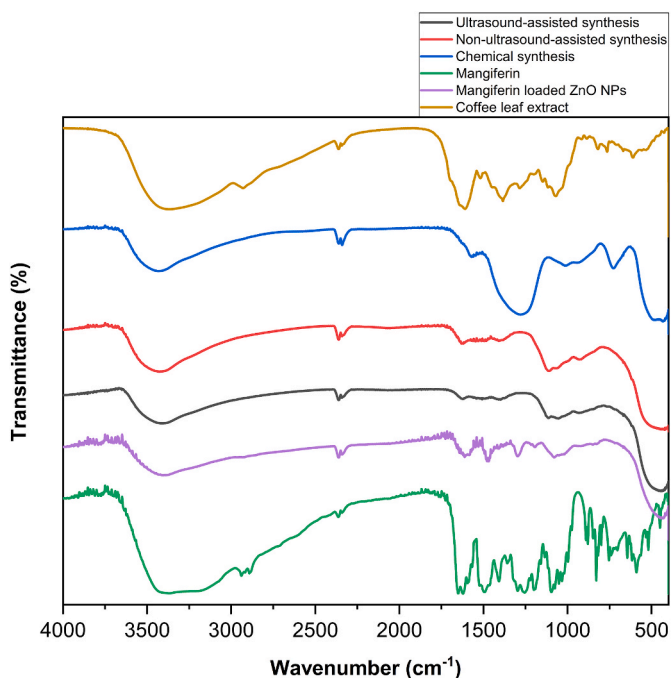
Fig. 5. XRD patterns for the ZnO NPs.

Fig. 6. FTIR spectrum of ZnO NPs.

78.52°, which corresponded to the planes of (100), (002), (101), (102), (110), (103), (200), (112), (201), (004) and (202), respectively. All noticed diffraction peaks were indexed to the hexagonal wurtzite structure (Bulcha et al., 2021). Furthermore, the observed sharp and narrow diffraction peaks indicated the good crystalline nature of synthesized ZnO NPs on all three methods.

3.4.5. FTIR analysis

FTIR was used to determine the functional groups of CLE and their role in the synthesis of ZnO NPs or plant metabolites present on the surface of NPs, which might be involved in the reduction and stabilization of NPs (Sankar et al., 2015). FTIR spectrum of ZnO NPs (Fig. 6) synthesized by US method exhibited a broad peak around 3340 cm^{-1}

corresponding to O–H stretching (Singh et al., 2009). Besides, the peaks at 1624 and 1452 cm^{-1} are related to C=C stretch and C–H bending vibrations, respectively (Cun et al., 2016). The FTIR spectrum of CLE showed peaks at 1315 and 617 cm^{-1}, indicating the presence of C–N stretch (aromatic amines) and alkyl halides (Ramimoghadam et al., 2012). The peaks at 1609, 1386 and 1071 cm^{-1} attribute to the N–H bending of amines, C–H stretching of alkanes and C–N stretching of aliphatic amines, respectively (Dhandapani et al., 2020). These peaks were shifted to 1624, 1397, and 1088 cm^{-1} in the case of US-ZnO NPs, which confirmed the successful formation of NPs using phytochemicals present in the CLE as reducing and stabilizing agents. Furthermore, the vibration of stretching peak appeared at 433 cm^{-1} corresponds to the characteristic peak of ZnO NPs, demonstrating the formation of ZnO NPs using US method. These observations were in good agreement with the previous study (Raghavendra et al., 2017). Similar results were observed for the synthesis of ZnO NPs using N-US method.

For the ZnO NPs synthesized using chemical method, the peak at 460 cm^{-1} corresponds to stretching vibration of ZnO NPs, which clearly indicates the formation of ZnO NPs (Mitra et al., 2012). The FTIR spectrum of the mangiferin showed major absorption peaks at 1545, 1494, 1340 and 1146 cm^{-1}. These peaks were also observed in the MGF-ZnO NPs, which confirmed the successful encapsulation of mangiferin on ZnO NPs.

3.4.6. Zeta potential analysis

The zeta potential is an ideal tool to identify the surface change and the stability of colloidal suspensions of NPs (Belay et al., 2017). The zeta potential values of the ZnO NPs synthesized by CLE with and without ultrasound treatment were 10.03 ± 0.50 mV and 6.19 ± 0.23 mV, respectively, which indicated that ultrasound-assisted synthesis of ZnO NPs could significantly improve the stability of ZnO NPs. Studies have shown that the cavitation effects of ultrasound and steric effect stabilized calcium zinc phosphate nanoparticles (Bhanvase and Sonawane, 2015). We also found that the zeta potential value of ZnO NPs synthesized by ultrasound before calcined was -23.84 ± 1.22 mV. The difference of zeta potential values between the NPs before and after calcining is because the negative organic molecules (e.g. OH-) loaded on the ZnO NPs were pyrolyzed due to the high temperature calcination. In addition, the MGF-ZnO NPs showed its zeta potential value of -15.79 ± 0.33 mV due to the OH- groups in the mangiferin which increased the repulsive force between ZnO NPs, thereby hindering agglomeration and improving their stability (Ali Dheyab et al., 2021).
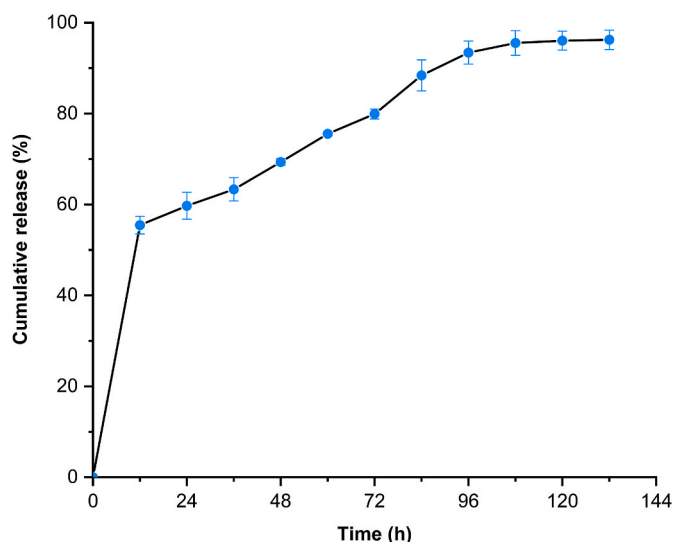

Fig. 7. Release profile of mangiferin loaded ZnO NPs.

3.5. In vitro mangiferin loading on and release from ZnO NPs

ZnO NPs have been used as nanocarriers for anticancer drugs or bioactive compounds such as doxorubicin, curcumin, and chlorogenic acid to increase the bioavailability and cytotoxicity of drugs (Singh et al., 2020). Mangiferin possesses various bioactivities, including antioxidant, anti-inflammatory, and anticancer activities (Mei et al., 2021a); however, the low bioavailability of mangiferin affects its efficacy. Therefore, scientists have encapsulated mangiferin in various nanoparticles to enhance its bioavailability and bioactivities (Aboyewa et al., 2021; Mei et al., 2021b). In the present study, we loaded mangiferin on the as-prepared ZnO NPs synthesized using CLE under ultrasonication. The loading and encapsulation efficiencies of mangiferin in ZnO NPs were $3.66 \pm 0.35\%$ and $19.01 \pm 1.90\%$, respectively. The reason for the low loading and encapsulation efficiencies may be due to the low mangiferin to ZnO NPs ratio used and the loss of mangiferin during extensive washing. To find the responsive release behavior of mangiferin, the drug release under pH 7.4 was explored. Fig. 7 showed the accumulated release of mangiferin at 37 °C over a period of 132 h. Mangiferin was released faster at the first 12 h and then the release rate was gradually slowed down as the time extended. After 120 h, the release of mangiferin reached plateau. The cumulative release percentage of mangiferin at 12, 84, 120 and 132 h were 55.46 ± 2.06, 88.41 ± 3.25, 96.05 ± 1.92 and $96.24 \pm 1.90\%$, respectively. These results proved that the MGF-ZnO NPs had good sustained-release properties. It is known that the drugs released in the fast release phase could quickly treat the disease, and the drugs in the slow-release phase could be used to consolidate the efficacy (Vimala et al., 2014). Mangiferin was loaded on ZnO NPs to achieve the effect of long-term release of drugs, which could reduce the side effects of drugs on human body. It could be reasonably inferred that the synthesized ZnO NPs using ultrasound-assisted method could be used as efficient nanocarriers and can be used as a new dosage form.

4. Conclusions

Green synthesis of NPs has been a highly attractive research area. This study reported an eco-friendly approach for the synthesis of ZnO NPs. In this study, CLE was used as a reducing, capping, stabilizing, and chelating agent for the synthesis of ZnO NPs via ultrasound-assisted method and the results were compared with non-ultrasound-assisted and chemical synthesis method. This synthesis method was simple, fast, effective and environmentally friendly, which was better than the conventional chemical method. The yield of ZnO NPs obtained under the optimum condition in combination with ultrasound and CLE was $43.59 \pm 0.13\%$, significantly higher than the non-ultrasound-assisted or the chemical methods. In addition, ultrasound treatment could significantly reduce the particle size and increase the stability of the synthesized ZnO NPs. Phenolic compounds, especially 5-CQA may be the major reducing and chelating agents for the synthesis of ZnO NPs. Mangiferin was successfully loaded on ZnO NPs and it achieved the effect of long-term release of bioactive. Therefore, we could reasonably predict that the ZnO NPs synthesized by green method could be used as efficient drug or bioactive carriers for further research.

CRediT authorship contribution statement

Qiang Wang: Experimental design, Investigation, Methodology, Data Formal analysis, Writing – original draft. **Suhuan Mei:** Investigation. **Perumal Manivel:** Writing – review & editing. **Haile Ma:** Resources. **Xiumin Chen:** Conceptualization, Experimental design, Supervision, Funding acquisition, Writing – original draft, Writing – review & editing.

Declaration of competing interest

The authors declare that they have no known competing financial interests or personal relationships that could have appeared to influence the work reported in this paper.

References

Aboyewa, J.A., Sibuyi, N.R.S., Meyer, M., Oguntibeju, O.O., 2021. Gold nanoparticles synthesized using extracts of *Cyclopia intermedia*, commonly known as honeybush, amplify the cytotoxic effects of doxorubicin. Nanomaterials 11, 132. https://doi.org/10.3390/nano11010132.

Ahmed, S., Annu, Chaudhry, S.A., Ikram, S., 2017. A review on biogenic synthesis of ZnO nanoparticles using plant extracts and microbes: a prospect towards green chemistry. J. Photochem. Photobiol. B Biol. 166, 272–284. https://doi.org/10.1016/j.jphotobiol.2016.12.011.

Ali Dheyab, M., Abdul Aziz, A., Jameel, M.S., Moradi Khaniabadi, P., Mehrdel, B., 2021. Sonochemical-assisted synthesis of highly stable gold nanoparticles catalyst for decoloration of methylene blue dye. Inorg. Chem. Commun. 127, 108551. https://doi.org/10.1016/j.inoche.2021.108551.

Alia, K., Dwivedi, S., Azam, A., Saquib, Q., Al-Said, M.S., Alkhedhairy, A.A., Musarrat, J., 2016. *Aloe vera* extract functionalized zinc oxide nanoparticles as nanoantibiotics against multi-drug resistant clinical bacterial isolates. J. Colloid Interface Sci. 472, 145–156. https://doi.org/10.1016/j.jcis.2016.03.021.

Álvarez-Chimal, R., García-Pérez, V.I., Álvarez-Pérez, M.A., Arenas-Alatorre, J.Á., 2021. Green synthesis of ZnO nanoparticles using a *Dysphania ambrosioides* extract. Structural characterization and antibacterial properties. Mater. Sci. Eng. C 118, 111540. https://doi.org/10.1016/j.msec.2020.111540.

Bandeira, M., Giovanela, M., Roesch-Ely, M., Devine, D.M., Da Silva Crespo, J., 2020. Green synthesis of zinc oxide nanoparticles: a review of the synthesis methodology and mechanism of formation. Sustain. Chem. Pharm. 15, 100223. https://doi.org/10.1016/j.scp.2020.100223.

Basnet, P., Inakhunbi Chanu, T., Samanta, D., Chatterjee, S., 2018. A review on bio-synthesized zinc oxide nanoparticles using plant extracts as reductants and stabilizing agents. J. Photochem. Photobiol., B 183, 201–221. https://doi.org/10.1016/j.jphotobiol.2018.04.036.

Belay, A., Kim, H.K., Hwang, Y.H., 2017. Spectroscopic study of binding of chlorogenic acid with the surface of ZnO nanoparticles. Russ. J. Phys. Chem. A. 91, 1781–1790. https://doi.org/10.1134/S0036024417090023.

Bhanvase, B.A., Sonawane, S.H., 2015. Effect of type and loading of surfactant on ultrasound-assisted synthesis of CaZn₂(PO4)₂ nanoparticles by chemical precipitation. Chem. Eng. Process 95, 347–352. https://doi.org/10.1016/j.cep.2015.07.017.

Bulcha, B., Leta Tesfaye, J., Anatol, D., Shanmugam, R., Dwarampudi, L.P., Nagaprasad, N., Bhargavi, V.L.N., Krishnaraj, R., 2021. Synthesis of zinc oxide nanoparticles by hydrothermal methods and spectroscopic investigation of ultraviolet radiation protective properties. J. Nanomater. 8617290. https://doi.org/10.1155/2021/8617290, 2021.

Chaudhuri, S.K., Malodia, L., 2017. Biosynthesis of zinc oxide nanoparticles using leaf extract of *Calotropis gigantea*: characterization and its evaluation on tree seedling growth in nursery stage. Appl. Nanosci. 7, 501–512. https://doi.org/10.1007/s13204-017-0586-7.

Chen, L., Xu, J., Tanner, D.A., Phelan, R., Van der Meulen, M., Holmes, J.D., Morris, M.A., 2009. One-step synthesis of stoichiometrically defined metal oxide nanoparticles at room temperature. Chem. Eur J. 15, 440–448. https://doi.org/10.1002/chem.200800992.

Chen, L., Xu, J., Holmes, J.D., Morris, M.A., 2010. A facile route to ZnO nanoparticle superlattices: synthesis, functionalization, and self-assembly. J. Phys. Chem. C 114, 2003–2011. https://doi.org/10.1021/jp9085766.

Chen, X., Ma, Z., Kitts, D.D., 2018. Effects of processing method and age of leaves on phytochemical profiles and bioactivity of coffee leaves. Food Chem. 249, 143–153. https://doi.org/10.1016/j.foodchem.2017.12.073.

Chen, X., 2019. A review on coffee leaves: phytochemicals, bioactivities and applications. Crit. Rev. Food Sci. Nutr. 59, 1008–1025. https://doi.org/10.1080/10408398.2018.1546667.

Chen, X., Tait, A.R., Kitts, D.D., 2017. Flavonoid composition of orange peel and its association with antioxidant and anti-inflammatory activities. Food Chem. 218, 15–21. https://doi.org/10.1016/j.foodchem.2016.09.016.

Cun, T., Dong, C., Huang, Q., 2016. Ionothermal precipitation of highly dispersive ZnO nanoparticles with improved photocatalytic performance. Appl. Surf. Sci. 384, 73–82. https://doi.org/10.1016/j.apsusc.2016.05.008.

Dhandapani, K.V., Anbumani, D., Gandhi, A.D., Annamalai, P., Muthuvenkatachalam, B.S., Kavitha, P., Ranganathan, B., 2020. Green route for the synthesis of zinc oxide nanoparticles from *Melia azedarach* leaf extract and evaluation of their antioxidant and antibacterial activities. Biocatal. Agric. Biotechnol. 24, 101517. https://doi.org/10.1016/j.bcab.2020.101517.

Duan, H., Wang, D., Li, Y., 2015. Green chemistry for nanoparticle synthesis. Chem. Soc. Rev. 44, 5778–5792. https://doi.org/10.1039/C4CS00363B.

Fu, L., Fu, Z., 2015. *Plectranthus amboinicus* leaf extract-assisted biosynthesis of ZnO nanoparticles and their photocatalytic activity. Ceram. Int. 41, 2492–2496. https://doi.org/10.1016/j.ceramint.2014.10.069.

Gao, Y., Xu, D., Ren, D., Zeng, K., Wu, X., 2020. Green synthesis of zinc oxide nanoparticles using *Citrus sinensis* peel extract and application to strawberry preservation: a comparison study. Lebensm. Wiss. Technol. 126, 109297. https://doi.org/10.1016/j.lwt.2020.109297.

Gupta, M., Tomar, R.S., Kaushik, S., Mishra, R.K., Sharma, D., 2018. Effective antimicrobial activity of green ZnO nano particles of Catharanthus roseus. Front. Microbiol. 9, 2030. https://doi.org/10.3389/fmicb.2018.02030.

Jamdagni, P., Khatri, P., Rana, J.S., 2018. Green synthesis of zinc oxide nanoparticles using flower extract of *Nyctanthes arbor-tristis* and their antifungal activity. J. King Saud Univ. Sci. 30, 168–175. https://doi.org/10.1016/j.jksus.2016.10.002.

Jayappa, M.D., Ramaiah, C.K., Kumar, M.A.P., Suresh, D., Prabhu, A., Devasya, R.P., Sheikh, S., 2020. Green synthesis of zinc oxide nanoparticles from the leaf, stem and *in vitro* grown callus of *Mussaenda frondosa* L.: characterization and their applications. Appl. Nanosci. 10, 3057–3074. https://doi.org/10.1007/s13204-020-01382-2.

Ji, D., Ma, H., Chen, X., 2021. Ultrasonication increases γ-aminobutyric acid accumulation in coffee leaves and affects total phenolic content and angiotensin-converting enzyme inhibitory activity. J. Food Process. Preserv. 45, e15777 https://doi.org/10.1111/jfpp.15777.

Khalil, M., Alqahtany, F.Z., 2020. Comparative studies of the synthesis and physical characterization of ZnO nanoparticles using *Nerium oleander* flower extract and chemical methods. J. Inorg. Organomet. 30, 3750–3760. https://doi.org/10.1007/s10904-020-01494-w.

Majumdar, D., 2019. Ultrasound-assisted Synthesis, Exfoliation and Functionalisation of Graphene Derivatives. Springer, Jeddah, pp. 63–103. https://doi.org/10.1007/978-981-32-9057-0_3.

Makino, K., Mossoba, M.M., Riesz, P., 1983. Chemical effects of ultrasound on aqueous solutions. Formation of hydroxyl radicals and hydrogen atoms. J. Phys. Chem. 87, 1369–1377. https://doi.org/10.1021/j100231a020.

Matinise, N., Fuku, X.G., Kaviyarasu, K., Mayedwa, N., Maaza, M., 2017. ZnO nanoparticles via Moringa *oleifera* green synthesis: physical properties & mechanism of formation. Appl. Surf. Sci. 406, 339–347. https://doi.org/10.1016/j.apsusc.2017.01.219.

Mei, S., Ma, H., Chen, X., 2021a. Anticancer and anti-inflammatory properties of mangiferin: a review of its molecular mechanisms. Food Chem. Toxicol. 149, 111997. https://doi.org/10.1016/j.fct.2021.111997.

Mei, S., Perumal, M., Battino, M., Kitts, D.D., Xiao, J., Ma, H., Chen, X., 2021b. Mangiferin: a review of dietary sources, absorption, metabolism, bioavailability, and safety. Crit. Rev. Food Sci. 1–19 https://doi.org/10.1080/10408398.2021.1983767.

Mitra, S., Patra, P., Chandra, S., Pramanik, P., Goswami, A., 2012. Efficacy of highly water-dispersed fabricated nano ZnO against clinically isolated bacterial strains. Appl. Nanosci. 2, 231–238. https://doi.org/10.1007/s13204-012-0095-7.

Mohanpuria, P., Rana, N.K., Yadav, S.K., 2008. Biosynthesis of nanoparticles: technological concepts and future applications. J. Nanoparticle Res. 10, 507–517. https://doi.org/10.1007/s11051-007-9275-x.

Nava, O.J., Soto-Robles, C.A., Gómez-Gutiérrez, C.M., Vilchis-Nestor, A.R., Castro-Beltrán, A., Olivas, A., Luque, P.A., 2017. Fruit peel extract mediated green synthesis of zinc oxide nanoparticles. J. Mol. Struct. 1147, 1–6. https://doi.org/10.1016/j.molstruc.2017.06.078.

Omran, B.A., Nassar, H.N., Fatthallah, N.A., Hamdy, A., El-Shatoury, E.H., El-Gendy, N. S., 2018. Waste upcycling of *Citrus sinensis* peels as a green route for the synthesis of silver nanoparticles. Energy Sources Part A. 40, 227–236. https://doi.org/10.1080/15567036.2017.1410597.

Osuntokun, J., Onwudiwe, D.C., Ebenso, E.E., 2019. Green synthesis of ZnO nanoparticles using aqueous *Brassica oleracea* L. var. *italica* and the photocatalytic activity. Green Chem. Lett. Rev. 12, 444–457. https://doi.org/10.1080/17518253.2019.1687761.

Pal, U., Kim, C.W., Jadhav, N.A., Kang, Y.S., 2009. Ultrasound-assisted synthesis of mesoporous ZnO nanostructures of different porosities. J. Phys. Chem. C 113, 14676–14680. https://doi.org/10.1021/jp904377n.

Perera, D.S.M., De Silva, R.C.L., Nayanajith, L.D.C., Colombage, H.C.D.P., Suresh, T.S., Abeysekera, W.P.K.M., Kottegoda, I.R.M., 2021. Anti-inflammatory and antioxidant properties of Coffea arabica/reduced graphene oxide nanocomposite prepared by green synthesis. Mat. Sci. Res. India 18, 305–317. https://doi.org/10.13005/msri/180306.

Pinjari, D.V., Pandit, A.B., Mhaske, S.T., 2016. Ultrasound assisted green synthesis of zinc oxide nanorods at room temperature. Indian J. Chem. Technol. 23, 221–226.

Raghavendra, M., Yatish, K.V., Lalithamba, H.S., 2017. Plant-mediated green synthesis of ZnO nanoparticles using *Garcinia gummi-gutta* seed extract: photoluminescence, screening of their catalytic activity in antioxidant, formylation and biodiesel production. Eur. Phys. J. Plus. 132, 358. https://doi.org/10.1140/epjp/i2017-11627-1.

Ramimoghadam, D., Hussein, M.Z.B., Taufiq-Yap, Y.H., 2012. The effect of sodium dodecyl sulfate (SDS) and cetyltrimethylammonium bromide (CTAB) on the properties of ZnO synthesized by hydrothermal method. Int. J. Mol. Sci. 13, 13275–13293. https://doi.org/10.3390/ijms131013275.

Sachdeva, A., Singh, S., Singh, P.K., 2021. Synthesis, characterisation and synergistic effect of ZnO nanoparticles to antimicrobial activity of silver nanoparticle. Mater. Today Proc. 34, 649–653. https://doi.org/10.1016/j.matpr.2020.03.150.

Sangeetha, G., Rajeshwari, S., Venckatesh, R., 2011. Green synthesis of zinc oxide nanoparticles by aloe barbadensis miller leaf extract: structure and optical properties. Mater. Res. Bull. 46, 2560–2566. https://doi.org/10.1016/j.materresbull.2011.07.046.

Sankar, R., Rizwana, K., Shivashangari, K.S., Ravikumar, V., 2015. Ultra-rapid photocatalytic activity of *Azadirachta indica* engineered colloidal titanium dioxide nanoparticles. Appl. Nanosci. 5, 731–736. https://doi.org/10.1007/s13204-014-0369-3.

Selim, Y.A., Azb, M.A., Ragab, I., Abd El-Azim, H.M., M, 2020. Green synthesis of zinc oxide nanoparticles using aqueous extract of *Deverra tortuosa* and their cytotoxic activities. Sci. Rep-Uk. 10, 3445. https://doi.org/10.1038/s41598-020-60541-1.

Sharifalhoseini, Z., Entezari, M.H., Shahidi, M., 2018. Sonication affects the quantity and the morphology of ZnO nanostructures synthesized on the mild steel and changes the corrosion protection of the surface. Ultrason. Sonochem. 41, 492–502. https://doi.org/10.1016/j.ultsonch.2017.10.012.

Singh, A.K., Viswanath, V., Janu, V.C., 2009. Synthesis, effect of capping agents, structural, optical and photoluminescence properties of ZnO nanoparticles. J. Lumin. 129, 874–878. https://doi.org/10.1016/j.jlumin.2009.03.027.

Singh, T.A., Das, J., Sil, P.C., 2020. Zinc oxide nanoparticles: a comprehensive review on its synthesis, anticancer and drug delivery applications as well as health risks. Adv. Colloid Interfac. 286, 102317. https://doi.org/10.1016/j.cis.2020.102317.

Sutradhar, P., Saha, M., 2016. Green synthesis of zinc oxide nanoparticles using tomato (*Lycopersicon esculentum*) extract and its photovoltaic application. J. Exp. Nanosci. 11, 314–327. https://doi.org/10.1080/17458080.2015.1059504.

Vimala, K., Sundarraj, S., Paulpandi, M., Vengatesan, S., Kannan, S., 2014. Green synthesized doxorubicin loaded zinc oxide nanoparticles regulates the Bax and Bcl-2 expression in breast and colon carcinoma. Process Biochem. 49, 160–172. https://doi.org/10.1016/j.procbio.2013.10.007.

Wang, D., Cui, L., Chang, X., Guan, D., 2020. Biosynthesis and characterization of zinc oxide nanoparticles from *Artemisia annua* and investigate their effect on proliferation, osteogenic differentiation and mineralization in human osteoblast-like MG-63 Cells. J. Photochem. Photobiol., B 202, 111652. https://doi.org/10.1016/j.jphotobiol.2019.111652.

Wang, X., Cao, Y., 2020. Characterizations of absorption, scattering, and transmission of typical nanoparticles and their suspensions. J. Ind. Eng. Chem. 82, 324–332. https://doi.org/10.1016/j.jiec.2019.10.030.